Korean J. Chem. Eng., 40(6), 1529-1539 (2023)
DOI: 10.1007/s11814-023-1376-4

pISSN: 0256-1115
eISSN: 1975-7220

Effect of cohesive particle addition on bubbling characteristics of gas-solid fluidized bed: Meso-scale mechanism

Liping Wei*,,†, Haoqi Li*, Changsong Wu***, Youjun Lu****, and Kun Luo*****,†**

*School of Chemical Engineering, Northwest University, Xi'an, Shaanxi 710069, China
**Xi'an Key Laboratory of Special Energy Materials, Northwest University, Xi'an, Shaanxi 710069, China
***École supérieure de physique et de chimie industrielles de la Ville de Paris, ESPCI Paris, 75005, France
****State Key Laboratory of Multiphase Flow in Power Engineering (SKLMF), Xi'an Jiaotong University, Xi'an, Shaanxi 710049, China
*****State Key Laboratory of Clean Energy Utilization, Zhejiang University, Hangzhou 310027, China
(*Received 20 September 2022 • Revised 2 December 2022 • Accepted 16 December 2022*)

Abstract−Due to the small particle size and large specific surface area, the cohesive particles affect the flow characteristics in a gas-solid bubbling fluidized bed. They can easily produce agglomerated and smooth heterogeneous flow under the different cohesive particle addition amounts. The influence of the cohesive particle amount on the bubbling characteristics was experimentally investigated for two typical cases: bed surface agglomerate and well-dispersed with the bed. The images of bubble rise were recorded by digital camera and processed by binarization to track bubble motion and obtained the bubble motion characteristics. An energy minimization multiscale (EMMS) model based on binary particle bubble was expanded to the flow of cohesive particles to reveal the basic mechanism of influence of the cohesive particle. By comparing the results predicted by the model with the experimental data, it is found that the change rules of bubble size and bubble rising speed are similar, which proves the feasibility of the newly developed EMMS model. A study of the structure shows that the addition of cohesive particles increases the size of the bubbles and inhibits the collapse of the bubble due to the reduction of the gas-solid resistance coefficient.

Keywords: EMMS Model, Cohesive Particles, Binary Particles, Bubbling System, Fluidized Bed

INTRODUCTION

As a reactor with high efficiency of mass transfer and heat transfer, the fluidized bed has been widely used in petroleum processing, metallurgy, chemical industry, energy and other industrial fields [1,2]. In practical production, a cohesive fine powder is always generated under physical and chemical effects, such as wear, collision, fracture, and reaction in a fluidized bed. When cohesive particles are mixed with bed materials, it will affect the bubbling behavior in the fluidized bed, and then affect the fluidization quality and chemical reaction process. Zhou and Li [3] showed that the size of cohesive particles has a great influence on fluidization, and the cohesion between particles increases with the reduction of particle size, which makes smaller particles more difficult to fluidize. Luo et al. [4] developed an EMMS model based on bubbles by considering the cohesive force on particle agglomerates. They found that adding cohesive particles increases the complexity of gas-solid fluidity due to cohesive particle agglomeration and breakage. Han et al. [5] found that adding lighter and smaller particles to binary components reduces the drag force of falling heavy particles needed to overcome, reducing the bubble diameter. Yates and Newton [6] found that the addition of fine particles to the fluidized bed increases the gas flow through the emulsified phase, reduces the bubble size, and increases the bed conversion. Zou et al. [7] found that in the fluidized bed, the bubble size generated by cohesive particles is smaller than that generated by category A & B particles, and it remains constant above a certain bed height, because the bubbles accumulate and disintegrate into a stable state under the influence of cohesive particles. The effect of cohesive particles on fluidization can be seen to be relatively complex, and its functional mechanism is still unclear.

Although many experimental investigations show the obvious effect of the cohesive particle addition, the basic models that can explain the phenomenon are still not achieved. The behavior of bubbles in fluidized bed can be represented by characteristic parameters, such as bubble size, bubble fraction, bubble rising velocity, and bubble dynamic wave velocity [8,9], which can be calculated by theoretical models and empirical correlations. Shi et al. [10] proposed a gas-solid bubbling EMMS model based on the EMMS theory [11], which can effectively describe the flow characteristics in a gas-solid bubbling fluidized bed. The bubble-based EMMS model is established by describing the fluidized bed bubbling system in three-scales, that is microscale of fluid-particle interaction between emulsion phase and bubble phase, the mesoscale of interphase in emulsion phase and bubble phase, and the macroscale of motion across the bed. The bubble-based EMMS model provides an effective tool for calculating bubble characteristic parameters, which can fully describe the bubbling system in a steady or non-

†To whom correspondence should be addressed.
E-mail: weiliping@nwu.edu.cn, zjulk@zju.edu.cn

steady state, so the model was enriched by multiple research groups to adapt to specific conditions [12-14].

Up to now, the bubble-based EMMS model is often used for the analysis of binary particle bubbling systems. Ahmad et al. [15, 16] extended the EMMS-bubbling model to fluidization studies of binary mixed particles based on the bubble diameter correlation [17]. Wang et al. [18] established a double-dispersion EMMS resistance model considering bubble effect under the assumption that there is no particle in the bubble. An EMMS model based on binary particle bubble was established by Wei and Lu [19] considering the influence of the interaction between the bubbles and the emulsion phase on the particle force balance within the emulsion phase. However, these models are not applicable to binary cohesive particle systems, which makes it difficult to understand the basic mechanism of the effect of adding cohesive particles on fluidization.

In this paper, a two-dimensional fluidized bed is used to study the effect and mechanism of adding cohesive particles on bubble characteristics. Although the flow characteristics of the two-dimensional fluidized bed are different from those of the three-dimensional fluidized bed, it still has certain reference value for the verification of some models. The behavior of bubble when the proportion of cohesive particles in binary particles changes is recorded experimentally, and the characteristic parameters of bubbles are calculated. At the same time, a bubble-based cohesive binary particle EMMS model is established, and the feasibility of the model is verified by comparing the bubble diameter obtained from the experiment and the model. Finally, the bubble behavior in the gas-solid bubbling system is predicted using the newly developed cohesive binary particle EMMS model.

EXPERIMENT AND DATA PROCESSING METHOD

1. Experiment

Fig. 1 shows the gas-solid fluidization experimental system, which consists of a Roots blower, a butterfly baffle, a ball valve, a flow meter, a gas chamber, and a fluidized bed. The Roots blower is used to provide the air source, and after the air enters the air chamber, the granular material is fluidized. The fluidized bed dimensions are width: 200 mm, height: 1,500 mm, and thickness: 15 mm. The height of the air chamber under the fluidized bed is set to 400 mm, which is high enough to filter the fluctuation of the intake air flow rate and achieve even airflow. A porous metal plate with a pore size of 30 μm is selected as the support structure for the material in the fluidized bed. The flow required for the experiment can be controlled by butterfly valve, ball valve, and flow meter. Differential pressure sensors (pressure range 0-5,000 Pa, high response frequency 1,000 Hz) are used to measure the air pressure in the bed. These sensors are installed on the sidewall of the fluidized bed at 50 mm, 150 mm, and 250 mm from the air distributor. The interface of the pressure connection tube is covered with a metal mesh with a porosity of fewer than 30 μm to prevent particles from entering the measuring tube and affecting the measurement accuracy. A digital camera (Nikon D330, 50 Hz) is used to record the bubble movement and shape in the fluidized bed. The scale is set on the bed, which can be used to determine the height of bed expansion and the location of bubble. The data acquisition system (NICompactDAQ-8174) was used to acquire air pressure data with a sampling rate of up to 200 kHz. Finally, uncertainty analysis of the experimental data is carried out to ensure that the uncertainty of flow rate and differential pressure is less than 0.2% and 0.25%, respectively.

The binary particles used in the experiment are quartz sand (Solid-phase 1) and corn powder (Solid-phase 2). The quartz sand used in the experiment has an equivalent diameter of 0.3-0.5 mm and density of 2,650 $kg \cdot m^{-3}$, belonging to Group-B. The corn powder has a diameter range of 3-25 μm and true density of 1,480 $kg \cdot m^{-3}$, which is a cohesive particle and belongs to Group-C. The size and shape of cohesive particles were measured with a digital microscope. The cohesive force and Young's modulus of particles

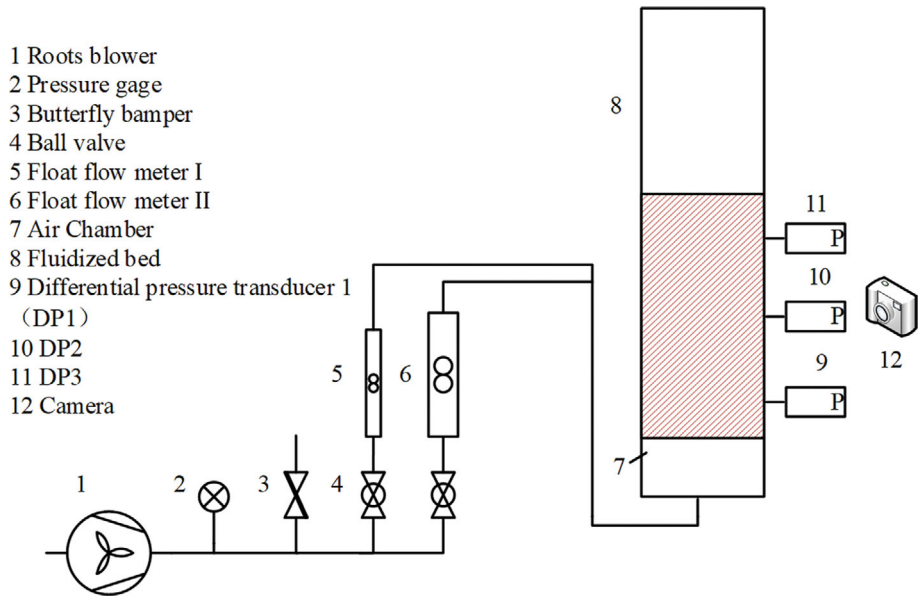

Fig. 1. Schematic diagram of the experimental device of the gas-solid fluidization system.

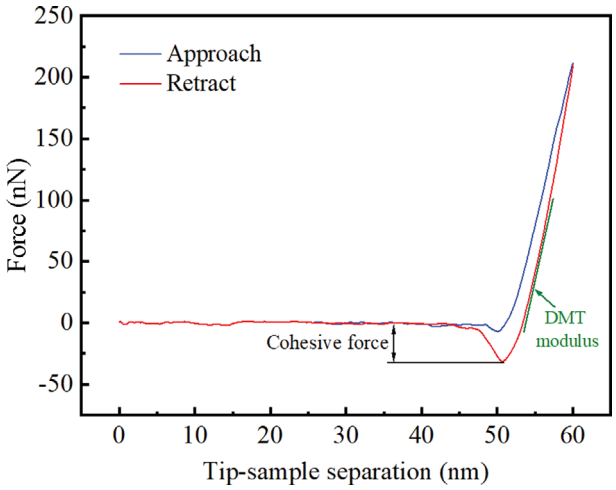

Fig. 2. Force-distance curve measured by AFM.

Table 1. Properties of the corn powder

Property	Corn powder	Unit
Projection area	135.09	μm^2
Circumference	44.05	μm
Sphericity	93.6%	-
Area equivalent diameter	13.12	μm
van der Waals force	31.34	nN
Young's modulus	60.836	GPa
Solid surface energy	0.059	J/m^2

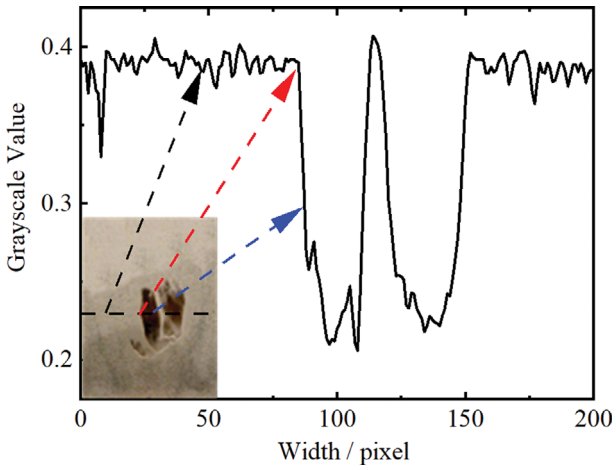

Fig. 3. The threshold determination method corresponding to the image (u_f=0.20 m·s^{-1}; cohesive particle proportion: 0 wt%).

could be evaluated with an atomic force microscope (AFM), as shown in Fig. 2. Cohesive force mainly includes van der Waals force and capillary force [20]. Because the particles used in the experiment are dry, the influence of capillary force is ignored in this study. The surface energy of particles is measured by contact angle/surface tension tester with two liquids of water and Hexadecane. Table 1 summarizes the properties of corn powder.

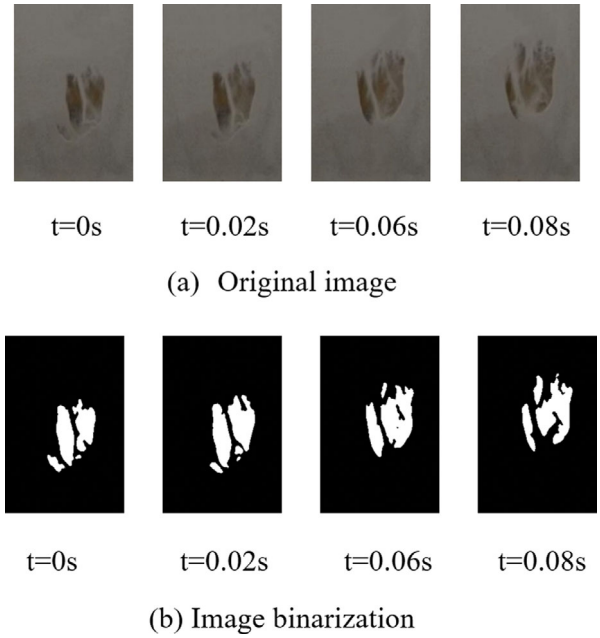

Fig. 4. An example of image processing results (u_f=0.20 m·s^{-1}; cohesive particle proportion: 0 wt%).

2. Data Analysis Method

In this experiment, images of the bubble are obtained with a camera. The bubble outlines can be determined by the pixel analysis of the middle line across the image. Fig. 3 shows the variation law of the grayscale value of a typical bubble image. The grayscale of bubble is far below that of the emulsion phase. By monitoring the turning point of the gray curves, the gray threshold value can be easily determined, and the turning point is between 0.31 and 0.35. The grayscale threshold is applied to convert the images to black-and-white binary images [21]. Then the images are denoised to remove the effects of noise. As shown in Fig. 4, the white area represents the bubble phase, and the black area represents the emulsified phase. Relatively regular and complete shapes are selected to study bubble characteristics, as shown in Fig. 3.

Based on the black-and-white binary images, the bubble size, aspect ratio, and rising velocity can be obtained. The bubble diameter can be calculated by the flood fill method [22]. When the solid fraction in the bubble is less than 0.2, the method can quickly identify the bubble cell and set it as the center. Then, based on the central unit, the flood filling algorithm obtains the bubble boundary by continuously expanding and calculating. The average coordinates of the bubble grid are selected as the coordinates of the center of mass of the bubbles.

$$x_b = \frac{\Sigma\Sigma x\Delta x\Delta y}{\Sigma\Delta x\Delta y} \quad (1)$$

$$y_b = \frac{\Sigma\Sigma y\Delta x\Delta y}{\Sigma\Delta x\Delta y} \quad (2)$$

where, x and y are the abscissa and ordinate of the bubble grid, Δx and Δy are the width and height of the single bubble grid, ΣΔxΔy represents the area of the bubble.

According to the bubble equivalent area, the bubble diameter d_b can be calculated.

$$d_b = \sqrt{\frac{4\Sigma\Delta x\Delta y}{\pi}} \tag{3}$$

The bubble aspect ratio R can be expressed as,

$$R = \frac{H_b}{L_b} \tag{4}$$

where, H_b is the maximum vertical height of the bubble, L_b is the maximum horizontal width of the bubble.

The bubble velocity can be divided into vertical and horizontal velocities. The bubble images of all corresponding moments can be obtained based on experiments. According to the centroid coordinates of bubbles corresponding to the continuous time, the velocity of bubbles can be calculated. Then, the bubble rising velocity is as follows:

$$u_b = \frac{y_b(t+\Delta t) - y_b(t)}{\Delta t} \tag{5}$$

In image processing, two continuous images are taken as a data group with a time interval of 0.02 s. According to the above binarization processing method, these images are processed by the image processing program, and then parameters like the rising velocity, size, and aspect ratio of bubbles are obtained.

BINARY EMMS MODEL FOR COHESIVE PARTICLE FLOW

1. Model Description

According to the EMMS theory, the typical binary bubbling fluidized system mainly contains a bubble phase, emulsion phase and interface phase [19]. The bubble phase is mainly formed by gas. Here, it is assumed that the bubble is composed entirely of gas, ignoring the effect of particles in bubble phase. Therefore, the physical properties of bubble phase are the same as those of the gas. The gas and particles are mixed to form the emulsion phase, and its properties are affected by particle size, density, and fraction. The interface phase is the manifestation of the interaction between the bubble phase and the emulsion phase. In this study, it is assumed that the bubble phase and emulsion phase are completely mixed. Then the binary EMMS model based on cohesive particles is described as follows.

The particle-gas mass balance equation and the bubble phase

Table 2. Particle-gas mass balance and bubble phase force balance equations

	Equations	
Mass equilibrium equations for particle and gas	$u_{s1} - u_{es1}(1-\chi) = 0$	(t1)
	$u_{s2} - u_{es2}(1-\chi) = 0$	(t2)
	$u_f - u_{ef}(1-\chi) - u_b\chi = 0$	(t3)
Bubble phase force equilibrium equation	$Cd_{eb} \cdot \frac{1}{2}\rho_e u_{eb}^2 \cdot \frac{\pi}{4} d_b^2 = (\rho_e - \rho_f)(g + a_b) \cdot \frac{\pi}{6} d_b^3$	(t4)
Bubble acceleration a_b	$a_b = \frac{\sigma^2[a_{es1}(\rho_{s1} - \rho_f) + a_{es1}(\rho_{s2} - \rho_f)]g}{C_b(1-\varepsilon_e)\chi\rho_e}$	(t5)
	$C_b = 0.5\left(\frac{1+2\chi}{1-\chi}\right)$	(t6)
	$\sigma^2 = \frac{(1-\varepsilon)^2\varepsilon^4}{1+4(1-\varepsilon)+4(1-\varepsilon)^2-4(1-\varepsilon)^3+(1-\varepsilon)^4}$	(t7)
Effective drag coefficient Cd_{eb}	$Cd_{eb} = Cd_i\|_{Re_{eb}}(1-\chi)^{-0.5}$	(t8)
	$Re_{eb} = \rho_e d_b u_{eb}/\mu_e$	(t9)
	$Cd_i = \begin{cases} 38Re_i^{-1.5} & 0 < Re_i \le 1.8 \\ 2.7 + 24/Re_i & Re_i > 1.8 \end{cases}$	(t10)
The slip velocity between the bubble and emulsion phases u_{eb}	$u_{eb} = (u_b - u_e)(1-\chi)$	(t11)
Superficial velocity of the emulsion phase u_e	$u_e = \frac{\rho_f u_{ef} + \rho_{s1} u_{es1} + \rho_{s2} u_{es2}}{\rho_e}$	(t12)
Density of the emulsion phase ρ_e	$\rho_e = \varepsilon_e\rho_f + \alpha_{es1}\rho_{s1} + \alpha_{es2}\rho_{s2}$	(t13)
Voidage of the emulsion phase ε_e	$\varepsilon_e = (\varepsilon - \chi)/(1-\chi)$	(t14)
Superficial slip velocity of particles 1 and 2 in the emulsion phase u_{efs}	$u_{efs1} = u_{ef} - \frac{\varepsilon_e}{\alpha_{es1}} u_{es1}$	(t15)
	$u_{efs2} = u_{ef} - \frac{\varepsilon_e}{\alpha_{es2}} u_{es2}$	(t16)

force balance equation in the fluidized bed have been described by the authors in previous work [19], and the details are shown in Table 2.

The cohesive particle force balance per unit volume in the emulsion phase: the sum of the drag force caused by the bubble-emulsion slippage, drag force caused by the gas-solid slippage in emulsion phase, cohesive force among cohesive particles, and cohesive force between cohesive particle phase and non-cohesive particle phase is equal to the effective weight of particles per unit volume. In contrast to cohesive particles, the force balance of non-cohesive particles is not affected by cohesive forces among cohesive particles. The bubble emulsion drag force of each solid phase is distributed to particle 1 and particle 2 according to the ratio of solid phase volume fraction.

$$150\frac{(1-\varepsilon_e)^2\mu_f}{\varepsilon_e^3}u_{ef}\left(\frac{\alpha_{es1}}{d_{s1}^2}+\frac{\alpha_{es2}}{d_{s2}^2}\right)+1.75\frac{(1-\varepsilon_e)\rho_f}{\varepsilon_e^3}u_{ef}^2\left(\frac{\alpha_{es1}}{d_{s1}}+\frac{\alpha_{es2}}{d_{s2}}\right)$$
$$=[\alpha_{es1}(\rho_{s1}-\rho_f)+\alpha_{es2}(\rho_{s2}-\rho_f)]$$
$$(1-\chi)g-(\rho_e-\rho_f)(g+a_b)+(1-\chi)(1-\varepsilon_e)F_c \quad (6)$$

where, α_{es1} is the solid fraction of particle 1 in emulsion phase, and α_{es2} is the solid fraction of particle 2 in emulsion phase, χ is the bubble fraction, and F_c is the cohesive force.

$$\alpha_{s1}=\alpha_{es1}(1-\chi) \quad (7)$$

$$\alpha_{s2}=\alpha_{es2}(1-\chi) \quad (8)$$

The cohesive force F_c can be calculated by the cohesive particle-particle interaction model [23]:

$$F_c=2(1+e')\frac{\rho_{s1}\alpha_{s1}\rho_{s2}\alpha_{s2}}{(\rho_{s1}d_{s1}^3+\rho_{s2}d_{s2}^3)}(d_{s1}+d_{s2})^2 g_{s1,s2}U_{s\_slip}^2 \quad (9)$$

where, $g_{s1,s2}$ is the radial distribution function of binary particles, which can be calculated by Eq. (10) [24]:

$$g_{s1,s2}=\frac{\left[(\alpha_{es1}+\alpha_{es2})^{1/3}+\frac{3}{4}(\alpha^*_{es1,es2})^{1/3}\right]}{(\alpha^*_{es1,es2})^{1/3}} \quad (10)$$

Fedors and Landel [25] presented the maximum solids volume fraction of the binary particle $\alpha^*_{es1,es2}$ under random packed conditions:

$$\alpha^*_{es1,es2}= \quad (11)$$
$$\begin{cases}\left[1-\left(\frac{d_{s1}}{d_{s2}}\right)^{0.5}\right](\alpha^*_{s1}-(1-\alpha^*_{s1})\alpha^*_{s2}) & \\ \left(1-\frac{\alpha_{es1}}{\alpha_{es1}+\alpha_{es2}}\right)+\alpha^*_{s1} & \frac{\alpha_{es1}}{\alpha_{es1}+\alpha_{es2}}\geq\frac{\alpha^*_{s1}}{\alpha^*_{s1}+(1-\alpha^*_{s2})\alpha^*_{s2}} \\ \left[(\alpha^*_{s1}-\alpha^*_{s2})+\left(\frac{d_{s1}}{d_{s2}}\right)^{0.5}(1-\alpha^*_{s1})\alpha^*_{s2}\right] & \\ [\alpha^*_{s1}-(1-\alpha^*_{s2})\alpha^*_{s1}]\frac{\alpha_{es1}}{(\alpha_{es1}+\alpha_{es2})\alpha^*_{s1}}+\alpha^*_{s2} & \frac{\alpha_{es1}}{\alpha_{es1}+\alpha_{es2}}<\frac{\alpha^*_{s1}}{\alpha^*_{s1}+(1-\alpha^*_{s2})\alpha^*_{s2}}\end{cases}$$

In Eq. (9), e′ is the modified coefficient of restitution after considering the effect of cohesive particles, which can be calculated by Eq. (12):

$$e'=e_{s1,s2}\sqrt{1-\frac{2m_0E_C}{m_{s1}m_{s2}e_{s1,s2}^2U_{s\_slip}^2}} \quad (12)$$

where, m_0 is the particle mass, E_C is the contact energy loss, and U_{s_slip} is the superficial slip velocity,

$$m_0=m_{s1}+m_{s2} \quad (13)$$

The superficial slip velocity U_{s_slip} [3] between solid-phase 1 and solid-phase 2 is an important parameter for determining the cohesive force between particles, which can be calculated by,

$$U_{s\_slip}=(1.5\overline{P}_{s,n}d_b g\varepsilon)^{0.5} \quad (14)$$

where, $\overline{P}_{s,n}$ is the dimensionless mean particle pressure for inviscid system, $\overline{P}_{s,n}\approx 0.077$ [3], and d_b is the bubble diameter, which can be calculated by the generalized bubble diameter correlation of Horio and Nonaka [27].

$$d_b=2.59g^{-0.2}[(u_f-u_{ef})A_t]^{0.4} \quad (15)$$

where, A_t is the bed cross-sectional area, m^2.

The contact energy loss E_C is caused by cohesion. which can be calculated by Eq. (13). Our previous work [26] described the contact energy in detail.

$$E_C=-\gamma\pi a'^2 \quad (16)$$

$$a'=\begin{cases}\left(\frac{9\pi}{2}\left(\frac{1-v^2}{E}\right)\gamma\left(\frac{d_p}{2}\right)^2\right)^{1/3} & \mu^*>1 \\ \left(\frac{3\pi}{4}\left(\frac{1-v^2}{E}\right)\gamma\left(\frac{d_p}{2}\right)^2\right)^{1/3} & \mu^*<1\end{cases} \quad (17)$$

$$\mu^*=\frac{32}{3\pi}\left[\frac{16\gamma^2}{\pi z_0^3}\left(\frac{1-v^2}{E}\right)^2 d_p\right]^{1/3} \quad (18)$$

where, a′ is the contact area radius of the particle, E is the Young modulus, $z_0\approx 0.3$ nm is the equilibrium separation between two solids [20]. v is the Poisson ratio.

Based on the calculation formula of van der Waals force F_v proposed by You and Wan, the relationship between contact energy loss and van der Waals force is obtained by combining it with Eq. (16):

$$F_v=\begin{cases}\left(\frac{1-v^2}{E}\right)^{-1}\frac{C_f^{3/2}}{3d_p}a'^3 & \mu^*>1 \\ \left(\frac{1-v^2}{E}\right)^{-1}\frac{8C_f^{3/2}}{3d_p}a'^3 & \mu^*<1\end{cases} \quad (19)$$

$$E_C=\begin{cases}-\gamma\pi\left(\frac{3d_pF_v}{C_f^{3/2}}\left(\frac{1-v^2}{E}\right)\right)^{2/3} & \mu^*>1 \\ -\gamma\pi\left(\frac{3d_pF_v}{8C_f^{3/2}}\left(\frac{1-v^2}{E}\right)\right)^{2/3} & \mu^*<1\end{cases} \quad (20)$$

where, C_f is the factor accounting for the percentage of nominal contact area, $C_f=1$ when the contact surface is smooth. The contact energy loss is 1.35×10-16 $kg\cdot m^2s^{-2}$ calculated by Eq. (20).

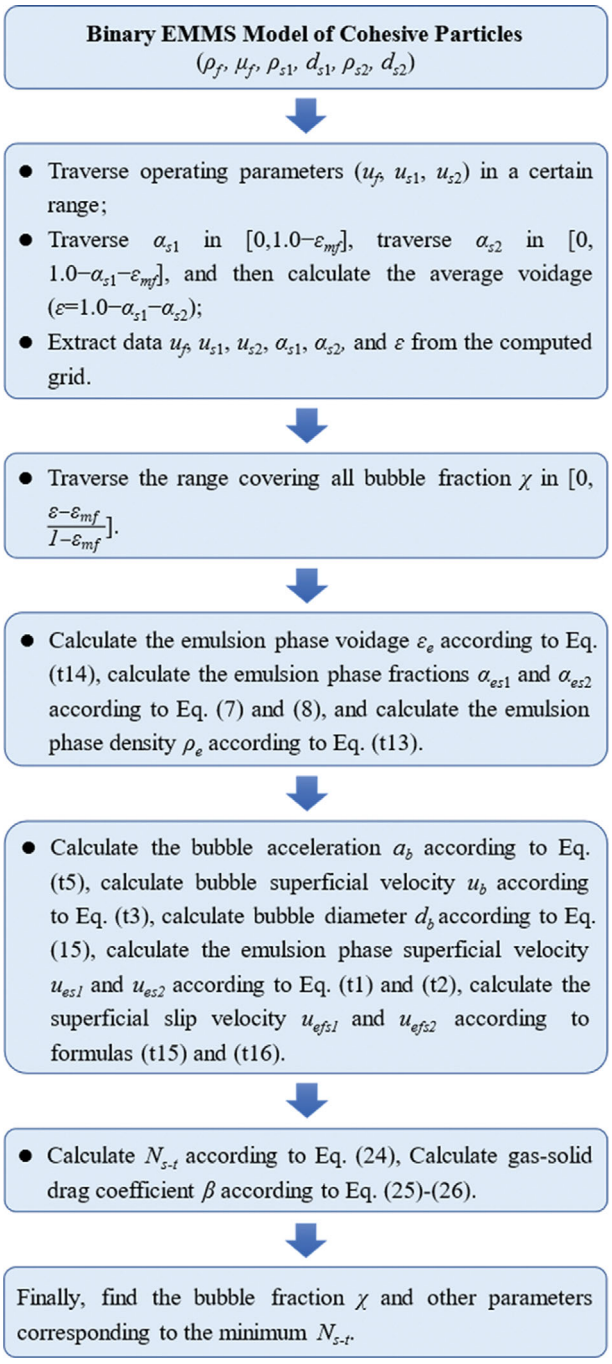

Fig. 5. Solving process of binary EMMS model equation system.

In this work, the system of equations needs to be closed by introducing a stability criterion (i.e., the minimization of the energy consumed per unit mass of particle suspension and transport) [11]. This energy consumption mainly includes the suspending energy consumed by binary particles suspended in emulsion phase and the transporting energy consumed when the emulsion phase transports bubbles. The bubble fraction is used as the metric to allocate the two-part energy, and the minimum energy consumption is achieved by choosing the bubble fraction [14,28]. Then, the energy consumption in the bubbling zone can be expressed as [14,19],

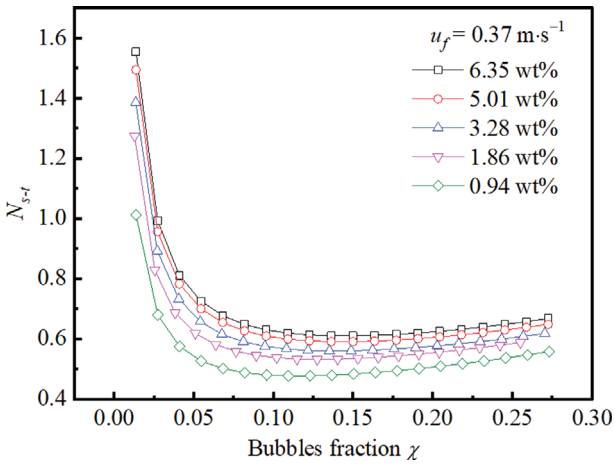

Fig. 6. Determination of the bubble fraction by the EMMS model.

$$N_{mse}=\left[\frac{\alpha_{s1}}{\rho_{s1}}\alpha_{es1}(\rho_{s1}-\rho_f)+\frac{\alpha_{s2}}{\rho_{s2}}\alpha_{es2}(\rho_{s2}-\rho_f)\right](1-\chi)g-(\rho_e-\rho_f)(g+a_b)u_{ef} \quad (21)$$

$$N_{msb}=\left[\frac{\alpha_{s1}}{\rho_{s1}}+\frac{\alpha_{s2}}{\rho_{s2}}\right](\rho_e-\rho_f)(g+a_b)u_b \quad (22)$$

$$N_t=\left(\frac{\alpha_{s1}}{\rho_{s1}}(\rho_{s1}-\rho_f)+\frac{\alpha_{s2}}{\rho_{s2}}(\rho_{s2}-\rho_f)\right)gu_f \quad (23)$$

$$N_{s-t}=(N_{mse}+N_{msb})N_t\rightarrow\min \quad (24)$$

The gas-solid drag coefficient can be expressed according to the original equations of the drag model by Gidaspow [29]:

$$\varepsilon\le0.8,\ \beta=150\frac{\alpha_s^2\mu_f}{\varepsilon d_s^2}+1.75\frac{\rho_s|u_s-u_f|}{d_s},\ s=s1,\ s2 \quad (25)$$

$$\varepsilon>0.8,\ \beta=\frac{3}{4}C_D\frac{\alpha_s\varepsilon\rho_s|u_s-u_f|}{d_s}\varepsilon^{-2.65},\ s=s1,\ s2 \quad (26)$$

$$C_D=\begin{cases}\frac{24}{\varepsilon Re_s}[1+0.15(\varepsilon Re_s)^{0.687}], & Re_s\le1000\\ 0.44, & Re_s\ge1000\end{cases} \quad (27)$$

$$Re_s=\frac{\alpha_s\rho_f d_p|u_s-u_f|}{\mu_f} \quad (28)$$

2. Model Solution

A detailed description of the computational scheme for solving the EMMS model equations is shown in Fig. 5.

Fig. 6 shows the relationship between N_{s-t} and bubble fraction. It can be found that N_{s-t} first decreases and then increases with the bubble fraction, and the bubble fraction corresponding to the minimum N_{s-t} can be found. The bubble fraction can be determined by the EMMS model. At the same time, the N_{s-t} increases with the increasing cohesive powder proportion.

RESULTS AND DISCUSSION

1. Effect of Cohesive Particle Addition on the Bubble Size

Fig. 7 shows the fluidization patterns of the bubbling fluidized

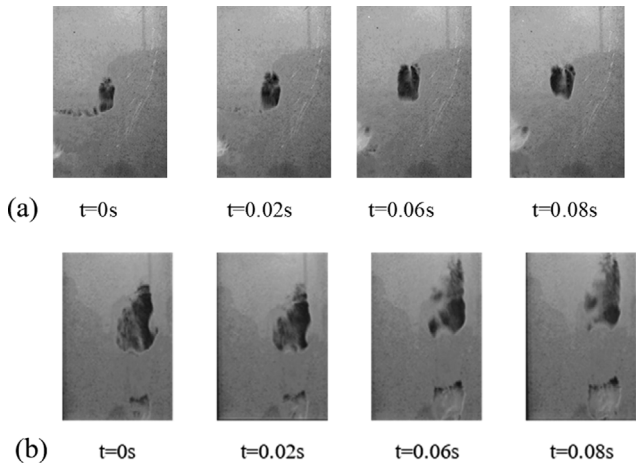

Fig. 7. Typical fluidization patterns of bubbling fluidized bed: (a) u_f= 0.20 m·s^{-1}, cohesive particle proportion: 0.94 wt%, surface agglomerate, (b) u_f=0.20 m·s^{-1}, cohesive particle proportion: 3.28 wt%.

bed in this experiment, as well as the evolution of bubbles. It can be seen that as the bubbles rise, they gradually grow larger. This is because in the rising process of the bubble, there is gas continuously entering the bubble from the emulsion phase, so that the bubble gradually grows during the rising process. When the bed material is not fully fluidized, the cohesive particles will aggregate on the surface of the bed, which seriously hinders the flow of gas and particles in the bed. This results in significantly smaller bubbles when the surfaces of cohesive particles are aggregated than when the particles are fully fluidized.

Fig. 8 shows the effect of agglomeration of cohesive particles on bubble size on the bed surface. It can be seen that the cohesive particles added in the initial state uniformly cover the bed surface and the medium in the bed in a layered arrangement. In the incomplete fluidization state, local agglomeration of cohesive particles is obvious, which hinders the flow of gas in the emulsion phase and reduces the bubble diameter. With the increase of the bed height, the bubble size almost fluctuates around 0.02 m, and there is no obvious increase trend.

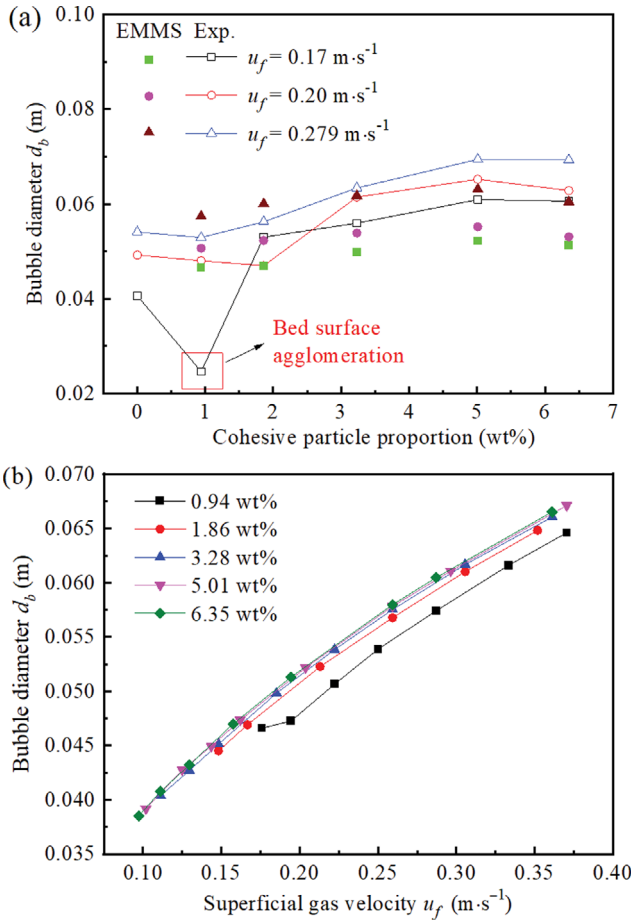

Fig. 9. The effect of adding cohesive particle on bubble size: (a) the effect of cohesive particle content, (b) the effect of superficial gas velocity.

Fig. 9(a) shows the variation of bubble diameter with the proportion of cohesive particles obtained by the model and experiment. As shown in the figure, the bubble diameter measured by the experiment is between 0.04-0.07 m. Comparing the experimental data with the prediction results of the EMMS model, it is found

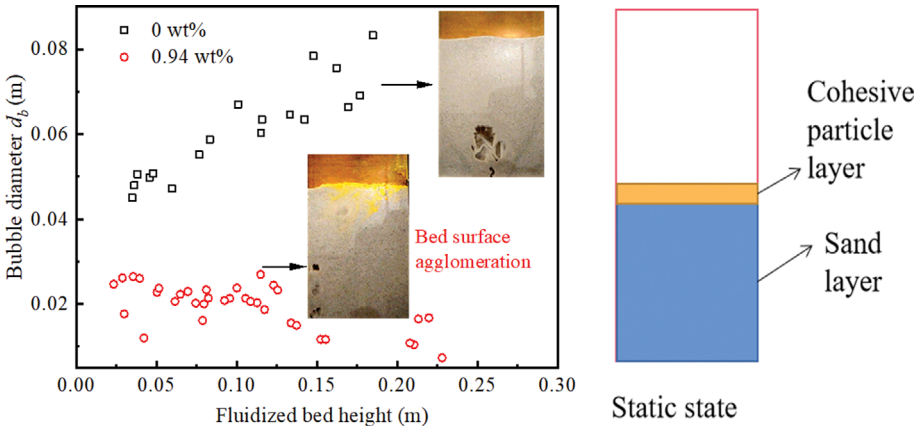

Fig. 8. Effect of bed surface agglomeration on bubble size and schematic diagram of initial state of binary particles.

that the variation trend of bubble diameter is similar. When the cohesive particles are uniformly mixed with the quartz sand, the bubble diameter increases slightly with the increase of the cohesive particle proportion, but when the cohesive particle proportion exceeds 5.01 wt%, the bubble diameter becomes slightly smaller. It may be that a small amount of cohesive particles reduce the gas-solid drag and promote the coalescence and growth of bubbles, but the effect is limited. When there are more cohesive particles, the coalescence and growth of bubbles will be hindered under the influence of cohesion. Notably, the bubble diameter is significantly reduced to 0.025 m when cohesive particles aggregate on the bed surface. Fig. 9(b) further shows the variation of bubble diameter with the superficial gas velocity. It can be seen that with the increase of the superficial gas velocity, the bubble diameter clearly increases. This is the same as the findings of Han et al. [5], and the reason may be that more gas leads to the merging of bubbles. Except for the curve with 0.94 wt% cohesive particles, the results of other curves are almost similar, which further shows that the increase of cohesive particles has little effect on bubble diameter.

2. Effect of Cohesive Particle Addition on the Bubble Fraction

Fig. 10 shows the change curve of voidage and bubble fraction with superficial gas velocity. The voidage is measured by experiment under different superficial gas velocities, and the bubble fraction is calculated by the binary EMMS model of cohesive particle flow established in this study. It is observed from the figure that the voidage and bubble fraction increase with the increase of the superficial gas velocity. However, the increasing trend of voidage and bubble fraction tends to be flat, when the superficial gas velocity is greater than 0.15 m^{-1}. This indicates that the effect of increasing superficial gas velocity the voidage and bubble fraction gradually decreases. With the increase of superficial gas velocity, the voidage values of different cohesive particle proportions are concentrated in a narrow range. However, the bubble fraction shows the opposite phenomenon, that the increase of cohesive particle proportions has little effect on the bed voidage, but increases the volume occupied by bubbles. The increase in cohesive particle reduces the mixture density of the bed material, which produces smaller resistant force for the gas flow and larger bubble fraction. The increasing cohesive particle seems to play an role for reducing the competition between solid-solid interaction and the gas-solid interaction.

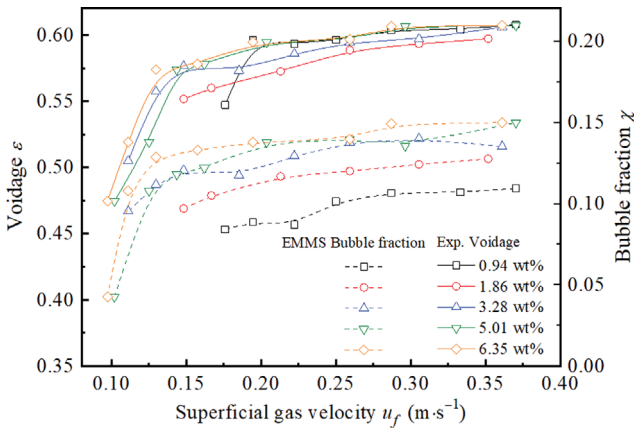

Fig. 10. The effect of superficial gas velocity on voidage and bubble fraction with different cohesive particle proportions.

3. Effect of Cohesive Particle Addition on the Bubble Rising Velocity

The cumulative distribution curve of the bubble rising velocity is shown in Fig. 11. Here, we count the bubble rising velocity when the bubble diameter is 0.04-0.06 m, and use P to represent the percentage of the number of bubbles whose rising speed is less than or equal to the corresponding speed on the abscissa in all bubbles. It is observed that the slope of the cumulative distribution curve decreases as the cohesive particle proportion increases, which indicates that the proportion of high-velocity bubbles increases with the cohesive particle proportions, and it also indicates that the cohesive particles increase the bubble rising velocity to a certain extent. Fig. 12 shows the variation of the bubble rising velocity with the bubble diameter. Generally speaking, the bubble rising velocity increases with the increase of bubble diameter. However, under different proportions of cohesive particles, the bubble rising velocity fluctuates in a wide range.

Literature [30] reviewed the variation law of bubble rising veloc-

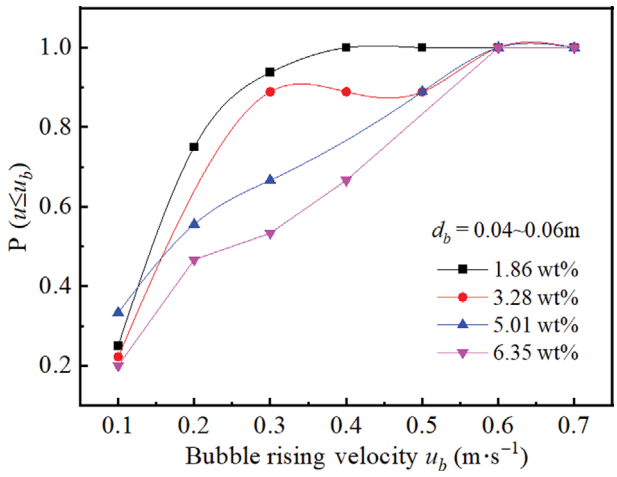

Fig. 11. The cumulative distribution of bubble rising velocity (u_f= 0.17-0.279 m·s^{-1}).

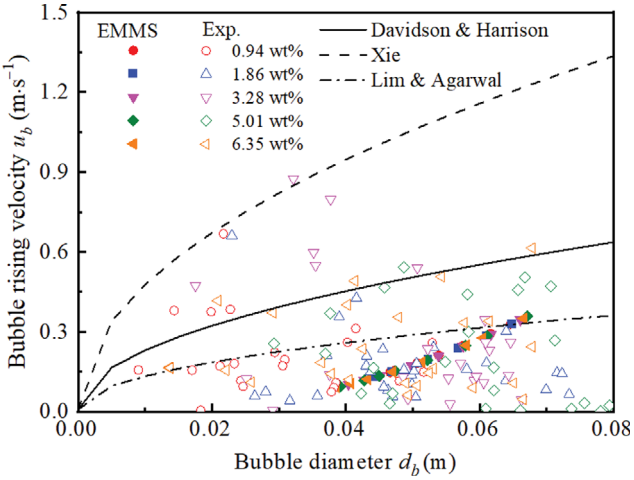

Fig. 12. The variation law between bubble rising velocity and bubble diameter (u_f=0.17-0.279 m·s^{-1}).

Table 3. Bubble rising velocity correlations

Authors	Expression	Literature
Karimipour	$u_b=(u_f-u_{mb})+\Phi(g\cdot d_b)^{1/2}$	[30]
Davidson & Harrison	$\Phi=0.71$	[31]
Xie	$\Phi=1.5$	[32]
Lim & Agarwal	$\Phi=0.4$	[33]

Table 4. The minimum bubbling velocity [34]

Cohesive particle proportion (wt%)	u_{b-min} (m/s)
0	0.162
0.94	0.153
1.86	0.139
3.28	0.111
5.01	0.102
6.35	0.097

ity with bubble diameter. The typical correlation function of bubble rising velocity and bubble diameter is shown in Table 3. The minimum bubbling velocity corresponding to different proportions of cohesive particles can be measured through experiments, and the values are listed in Table 4. According to the different correction coefficients reported in the literature [31-33], the variation between bubble rising velocity and bubble diameter can be calculated, as shown in Fig. 12. The very small value of the correction coefficient Φ of 0.4 suggested by Lim and Agarwal [33] has higher prediction accuracy. Both Davidson and Harrison's [31] correlation and Xie's [32] correlation predict higher rising velocities than the experimental data. Compared to Lim and Agarwal's [33] correlations, the EMMS model predicts a much lower bubble rising velocity when the bubble diameter is lower than 0.065 m, which is closer to the experimental results. This indicates that the EMMS model, as a system model, can be used to study the influence of cohesive particles. However, this study is based on the two-dimensional fluidized bed, so the model is limited to predicting the flow characteristics in the two-dimensional fluidized bed.

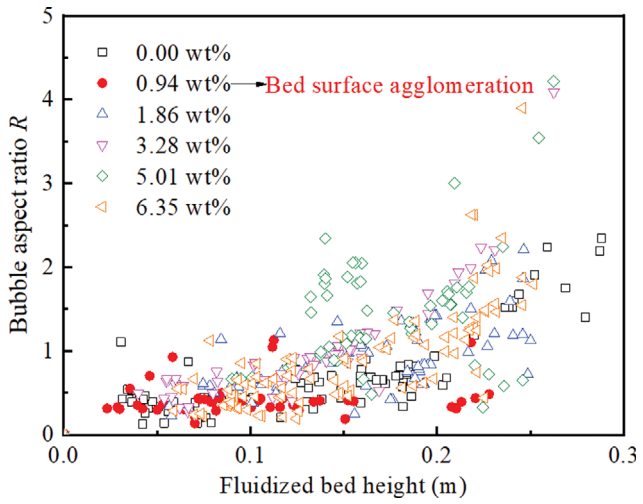

Fig. 13. Distribution of bubble aspect ratio values along with bed height (u_f=0.17 m·s^{-1}).

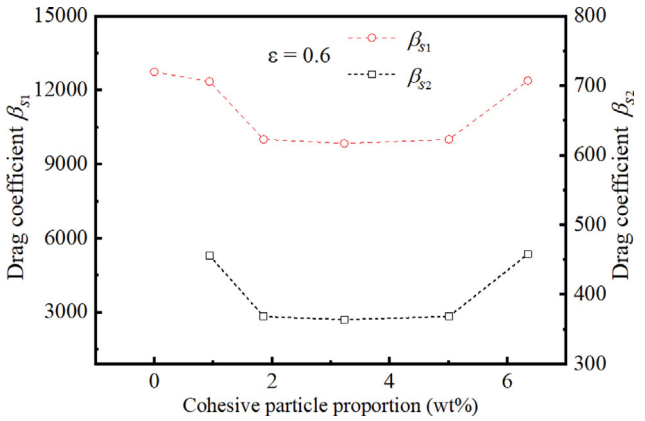

Fig. 14. Variation of drag coefficient with increasing proportions of cohesive particle (s1: quartz sand; s2: corn powder).

4. Effect of Cohesive Particle on Bubble Shape

Fig. 13 shows the variation law of the aspect ratio of bubbles generated by different cohesive particle proportions along the bed height direction. As the bed height increases, the bubbles gradually change from the flat ball at the bottom to the long and narrow ball. When the surface of the bed gathers cohesive particles, the bubble remains a flat spherical shape and the bubble aspect ratio slightly changes along with the bed height, as shown in Fig. 7(a). This is attributed to the cohesive particle agglomerate on the fluidized bed surface increasing the bubble's rise resistance. When the cohesive particles and bed materials are fully mixed, the bubble shape narrows with increasing proportion of cohesive particles, and as the bed height increases, the bubble aspect ratio also increases, as shown in Fig. 7(b). The reason is that the cohesive particles in the bubbling bed weaken the interaction of bubble phase with emulsion phase, thereby reducing bubble rupture and changing the shape of the bubbles. Fig. 14 further presents the drag coefficient of binary particles calculated by the EMMS model at different proportions of cohesive particle. It is clear that the calculated drag coefficient of the cohesive particle phase is lower than the sand solid particle due to the cohesive particle-phase having a lower particle fraction and density. The binary EMMS model validates that a solid phase with low solid fraction and low density suffers a lower drag force in a non-cohesive binary bubbling system [19]. The present results indicate that this conclusion is also suitable for the cohesive binary bubbling system when the cohesive particles are not agglomerated. Finally, it is observed that the variation law of the cohesive coefficient with the viscous particle proportion is to decrease first and then increase.

CONCLUSIONS

The influence of cohesive particles on bubble behavior in a binary bubble system was studied experimentally. Then, the bubble-based binary particle EMMS model was extended to cohesive particle flow, and the effect of cohesive particle-particle resistance on the binary particle force balance in the emulsion phase was considered. Finally, the influences of cohesive particle addition on the bubble

characteristics were analyzed from the aspects of bubble size, bubble fraction, bubble rising speed, and bubble shape. The conclusions are as follows:

(1) The EMMS model based on cohesive binary particle bubbles was validated by comparing the calculated bubble size and experimentally measured value. When the cohesive particle and sand were well mixed, both the experiment and the EMMS model showed the bubble size increased with the cohesive particle addition in the range of 0-5.01 wt%, while the bubble size slightly decreased when the cohesive particle proportion was over 5.01 wt%.
(2) Given the measured parameters of average bed voidage and superficial velocity, the EMMS model can predict bubble fraction, which is hardly measured by the experiments. The calculated bubble fraction increases with the increase of the proportion of cohesive particles. The EMMS model and Lim and Agarwal correlation can be used to predict the bubble rising velocity.
(3) The experiments show that the aspect ratio of bubbles increases with the increasing bed height when the cohesive particles and bed materials are well mixed, which is induced by the weakened bubble broken.

ACKNOWLEDGEMENTS

This work is currently supported by the National Natural Science Foundation of China through contract No. 22278332. Supported by the State Key Laboratory of Clean Energy Utilization (Open Fund Project No. ZJUCEU2020020).

NOMENCLATURE

a : acceleration ($m \cdot s^{-2}$)
a' : contact area radius of the particles
C_f : factor accounting for the percentage of nominal contact area
d : diameter [m]
e' : corrected coefficient of restitution
E : Young's modulus of solid
E_c : contact energy loss [$kg \cdot m^2 s^{-2}$]
F_c : cohesive force [N]
g : gravitational acceleration [$m \cdot s^{-2}$]
$g_{s1,s2}$: radial distribution function of binary particles
m_0 : particle mass
N_{mse} : suspending energy consumption
N_{msb} : transporting energy consumption
N_t : total suspending and transporting energy consumption
R : bubble aspect ratio
Re : Reynolds number
u : superficial velocity [$m \cdot s^{-1}$]
u_b : bubble rising velocity [$m \cdot s^{-1}$]
U_{s_slip} : superficial slip velocity between particles [$m \cdot s^{-1}$]
v : poisson ratio
z_0 : equilibrium separation between two solids

Greek Letters

α : solid fraction
$a^*_{es1,es2}$: maximum solids volume fraction of the binary particle
β : gas-solid drag coefficient
γ : solid surface energy per unit contact area
ε : voidage
ρ : density [$kg \cdot m^{-3}$]
μ : viscosity [Pa·s]
μ^* : dimensionless parameter
χ : bubbles fraction

Subscripts

b : bubble phase
e : emulsion phase
ef : fluid in emulsion phase
es1 : solid phase particle 1 of emulsion phase
es2 : solid phase particle 2 of emulsion phase
f : fluid
min : the minimum value
p : particle
s1 : solid phase particle 1
s2 : solid phase particle 2

REFERENCES

1. S. Pielsticker, B. Gövert, T. Kreitzberg, M. Habermehl, O. Hatzfeld and R. Kneer, *Fuel*, **190**, 420 (2017).
2. Y. Shao, W. Zhong and A. Yu, *Powder Technol.*, **304**, 73 (2016).
3. Z. Tao and H. Li, *Powder Technol.*, **101**, 57 (1999).
4. H. Luo, B. Lu, J. Zhang, H. Wu and W. Wang, *Chem. Eng. J.*, **326**, 47 (2017).
5. B. Han, The University of Western Ontario (2017).
6. J. G. Yates and D. Newton, *Chem. Eng. Sci.*, **41**, 801 (1986).
7. Z. Zou, H. Z. Li and Q. S. Zhu, *Powder Technol.*, **212**, 258 (2011).
8. L. Wei and Y. Lu, *Chem. Eng. Sci.*, **147**, 21 (2016).
9. L. Wei, Y. Lu, G. Jiang, J. Hu and J. Zhu, *Chem. Eng. Res. Des.*, **126**, 255 (2017).
10. Z. Shi, W. Wang and J. Li, *Chem. Eng. Sci.*, **66**, 5541 (2011).
11. J. Li and M. Kwauk, *Ind. Eng. Chem. Res.*, **40**, 4227 (2001).
12. K. Hong, Z. Shi, A. Ullah and W. Wang, *Powder Technol.*, **266**, 424 (2014).
13. S. Song, Z. Hao, L. Dong, J. Li and Y. Fang, *RSC Adv.*, **6**, 111041 (2016).
14. X. Liu, Y. Jiang, C. Liu, W. Wang and J. Li, *Ind. Eng. Chem. Res.*, **53**, 2800 (2014).
15. N. Ahmad, Y. Tian, B. Lu, K. Hong, H. Wang and W. Wang, *Chin. J. Chem. Eng.*, **27**, 54 (2019).
16. N. Ahmad, Y. Tong, B. Lu and W. Wang, *Chem. Eng. Sci.*, **200**, 257 (2019).
17. M. Horio and A. Nonaka, *AIChE J.*, **33**, 1865 (1987).
18. S. Wang, K. Zhang, S. Xu and X. Yang, *Powder Technol.*, **338**, 280 (2018).
19. L. Wei and Y. Lu, *Adv. Powder Technol.*, **31**, 1529 (2020).
20. S. You and M. P. Wan, *Langmuir*, **29**, 9104 (2013).
21. G. R. Caicedo, J. J. P. Marqués, M. G. a. Ruíz and J. G. Soler, *Chem. Eng. Process.*, **42**, 9 (2003).
22. Y. Lu, J. Huang and P. Zheng, *Chem. Eng. J.*, **274**, 123 (2015).
23. L. Wei, G. Jiang, H. Teng, J. Hu and J. Zhu, *Particuology*, **49**, 95

(2020).
24. R. A. Bell, Swinburne University of Technology (2000).
25. R. Fedors and R. Landel, *Powder Technol*., **23**, 225 (1979).
26. L. Wei, Y. Gu, Y. Wang and Y. Lu, *Powder Technol*., **364**, 264 (2020).
27. M. Horio and A. Nonaka, *AIChE J*., **33**, 1865 (1987).
28. J. Li, W. Ge, W. Wang, N. Yang, X. Liu, L. Wang, X. He, X. Wang, J. Y. Wang and M. Kwauk, *From multiscale modeling to meso-science: A chemical engineering perspective*, Springer. Publications, Berlin (2013).
29. D. Gidaspow, *J. Non-Newton. Fluid*., **55**, 207 (1994).
30. S. Karimipour and T. Pugsley, *Powder Technol*., **205**, 1 (2011).
31. J. F. Davidson and D. Harrison, Fluidization, Academic Press. Publications, London (1971).
32. H. Y. Xie, *Adv. Powder Technol*., **8**, 217 (1997).
33. K. S. Lim and P. K. Agarwal, *Powder Technol*., **69**, 239 (1992).
34. L. Wei, Y. Lu, J. Zhu, G. Jiang, J. Hu and H. Teng, *Korean J. Chem. Eng*., **35**, 2117 (2018).